Acta Mech 225, 2943–2957 (2014)
DOI 10.1007/s00707-014-1212-3

Y. Sapsathiarn · Y. Singh · R. K. N. D. Rajapakse

Numerical modelling of piezoelectric actuators exposed to hydrogen

Received: 9 September 2013 / Revised: 28 January 2014 / Published online: 31 July 2014

Abstract Modern fuel injectors have been developed based on piezoelectric stack actuators. Performance and durability of actuators in a hydrogen environment are important considerations in the development of hydrogen injectors. 2D plane stress and 3D models for analysis of coupled diffusion and thermo-electromechanical response of actuators are presented. Chemical potential, electric field and temperature gradients are taken as driving forces for hydrogen transport. The explicit Euler finite difference method is used to solve the nonlinear diffusion governing equation. The finite element method is used for time-dependent analysis of fully coupled mechanical, electric and thermal fields. The diffusion process and thermo-electromechanical deformations are coupled through the dependence of piezoelectric properties on hydrogen concentration. Experimental results for the piezoelectric coefficient d_{33} of PZT ceramics exposed to different hydrogen concentrations are used. A comparison of a fully coupled 2D model with 2D and 3D models with reduced coupling is made to examine the significance of coupling and computational efficiency. Selected numerical results are presented for time histories of hydrogen concentration, temperature and stroke of an idealized actuator unit cell to obtain a preliminary understanding of the performance of actuators exposed to hydrogen.

1 Introduction

Piezoelectric sensors and actuators are the key building blocks of smart materials and structures technology [1–3]. Recently, advanced fuel injectors that utilize multilayer piezoelectric actuators (Fig. 1) for injector needle opening have been introduced as an innovative alternative to conventional solenoid technology [4,5]. Piezo actuator-based fuel injectors represent a promising improvement in direct fuel injection technology with precise positioning and injection and rapid response time compared to conventional solenoid technology.

Clean energy sources are increasingly used for transportation due to environmental concerns and declining supply of fossil fuels. Hydrogen is a clean fuel that is free from carbon dioxide and other sources of greenhouse gas. Substantial R&D efforts have been taking place for over two decades to develop automobiles, heavy vehicles and stationary power systems based on hydrogen technology including fuel cells. There is strong

Presented at the Third Asian Conference on Mechanics of Functional Materials and Structures at the Indian Institute of Technology Delhi in New Delhi, India, December 5–8, 2012.

Y. Sapsathiarn (✉)
Department of Civil and Environmental Engineering, Mahidol University, Nakhon Pathom 73170, Thailand
E-mail: yasothorn.sap@mahidol.ac.th

Y. Singh · R. K. N. D. Rajapakse
Faculty of Applied Sciences, Simon Fraser University, Burnaby, V5A 1S6, Canada
E-mail: rajapakse@sfu.ca
Tel.: +1.778.782.3826
Fax: +1.778.782.5802

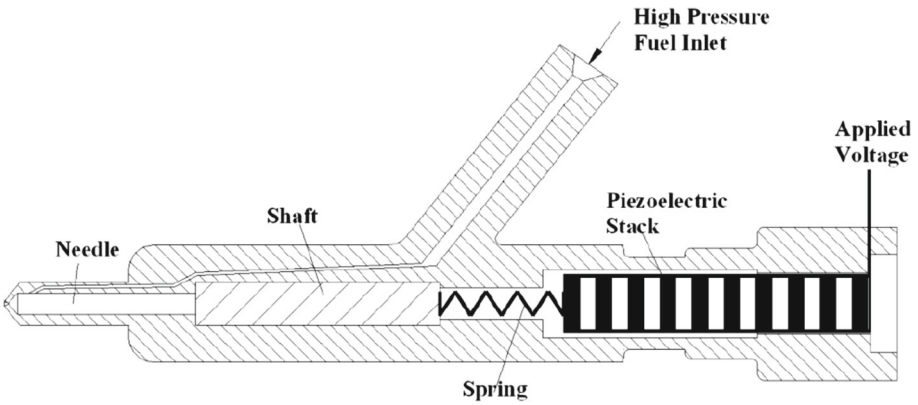

Fig. 1 Schematic of fuel injector with piezoelectric actuator

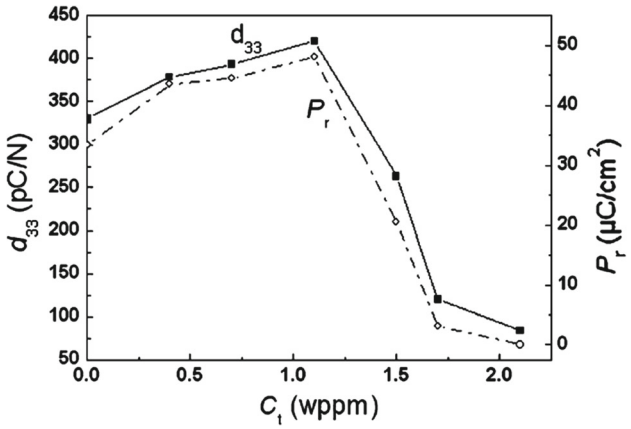

Fig. 2 Variation of piezoelectric properties with hydrogen concentration [6]

interest in the industry to extend the piezoelectric actuator technology for hydrogen fuel injectors. However, little is known about the performance of piezoelectric actuators in a hydrogen environment.

The effect of hydrogen on piezoceramic materials has received attention in recent years. Experiments by Wu et al. [6] suggest that piezoelectric properties of PZNT and PZT are strongly influenced by the diffused hydrogen content. The experimental results of Wu et al. [6] showing the dependence of piezoelectric constant d_{33} and remnant polarization P_r on hydrogen concentration are reproduced in Fig. 2. Peng et al. [7] observed that micro cracks/fissures initiate and grow discontinuously along grain boundaries of PZT due to hydrogen diffusion. Experiments by Wang et al. [8] showed that the strength and fracture toughness of PZT exposed to H_2 decrease linearly with the logarithm of hydrogen concentration. Recent studies by Shafiei et al. [9,10] reported that hydrogen-treated PZT has lower electrical resistance and higher capacitance as compared to as-received (hydrogen-free) PZT.

Study of the performance of piezoelectric stack actuators under conditions relevant to operation of automotive fuel injectors has received some attention in the literature. Li et al. [11] experimentally studied the quasi-static thermo-electromechanical performance of stack actuators and developed a simple mathematical model. Senousy et al. [12] experimentally investigated the dynamic behaviour of PZT stack actuators to understand the influence of driving frequency, electric field magnitude, rise time and duty cycle on stroke. Wang et al. [13] conducted cyclic fatigue tests on stack actuators and reported that a significant reduction in piezoelectric and dielectric behaviour during cycling. The above studies are concerned with actuators in a non-hydrogen environment.

Studies on the behaviour of stack actuators in hydrogen environments are still in the very early stages of development. For example, experimental studies of the hydrogen effect on the performance of stack actuators are being performed in the U.S. Department of Energy—Propulsion Materials Research and Development Program [14]. This paper presents details of a numerical model for analysis of hydrogen diffusion in and thermo-piezoelectric response of piezoelectric materials. A modified Cahn–Hilliard equation [15,16] is used

to describe the hydrogen diffusion process. The coupled thermo-piezoelectric governing equations are solved for the 2D plane stress case by coupling the finite element method with the nonlinear diffusion equation through the dependence of material properties on hydrogen concentration. The coupled 2D case is compared with a 2D model with reduced coupling based on the 'Equation Based Modelling' capability of *COMSOL Multiphysics*®. Selected numerical results for 2D and 3D cases are presented to understand the hydrogen diffusion process and thermo-piezoelectric response of a single stack in an actuator.

2 Field equations

The governing equations for the electro-thermo-mechanical response of a piezoelectric material are given by [17]

$$D_{i,i} - \Phi_e = 0; \quad q_{i,i} - \theta_s \dot{s} = \Phi_t; \quad \sigma_{ij,j} + b_i = \rho \ddot{u}_i, \tag{1}$$

where D_i, q_i and u_i are the electric displacement, heat flux and mechanical displacement in the ith-direction, respectively; σ_{ij} is the stress tensor; Φ_e, Φ_t and b_i are the electric body charge, heat source density and mechanical body force components, respectively; s is the entropy density; θ_s is the surrounding reference temperature, and ρ is the mass density.

The mechanical strain (ε_{ij}), electric field (E_i) and temperature (θ) are related to stress (σ_{ij}), electric displacement (D_i) and entropy density (s) by the following constitutive relations:

$$\sigma_{ij} = C_{ijkl}\varepsilon_{kl} - e_{kij}E_k - \lambda_{ij}\theta, \tag{2a}$$

$$D_i = e_{ijk}\varepsilon_{kj} + g_{ik}E_k + p_i\theta, \tag{2b}$$

$$s = \lambda_{kl}\varepsilon_{kl} + p_k E_k + \alpha_v \theta, \tag{2c}$$

where C_{ijkl}, e_{ikl}, g_{kl}, λ_{kl} and p_m are the elastic constants, piezoelectric constants, dielectric coefficients, thermal stress coefficients and pyroelectric constants, respectively; θ is the temperature increase from the stress-free state; and $\alpha_v = \rho C_v/\theta_s$ where C_v is the specific heat at constant volume.

In addition, the following basic relations exist:

$$\varepsilon_{ij} = \frac{1}{2}(u_{i,j} + u_{j,i}); \quad E_i = -\phi_{,i}; \quad q_i = -\kappa_{ij}\theta_{,j}, \tag{3}$$

where κ_{ij} is the thermal conductivity tensor and ϕ is the electric potential.

The admissible mechanical, electric and thermal boundary conditions on the boundary Γ are given by

$$\text{Mechanical}: \quad u_i = \bar{u}_i \quad \text{or} \quad \sigma_{ij}n_j = \bar{t}_i \tag{4a}$$

$$\text{Electric}: \quad \phi = \bar{V} \quad \text{or} \quad D_i n_i = -\bar{Q} \tag{4b}$$

$$\text{Thermal}: \quad \theta = \bar{\theta} \quad \text{or} \quad -\kappa_{ij}\theta_{,j}n_j = \bar{q} + h_v(\theta_f - \theta_s) \tag{4c}$$

where $\bar{u}_i$ and $\bar{t}_i$ are the specified mechanical displacement and surface traction components in the i-direction, respectively; n_i denotes components of outward unit normal vector to Γ; $\bar{V}$ and $\bar{Q}$ are the specified electric potential and surface charge; $\bar{\theta}$ and $\bar{q}$ are the prescribed temperature and rate of heat flow per unit area; θ_f is the ambient fluid temperature; and h_v is the convection heat transfer coefficient.

In view of Eqs. (1) and (3), Eq. (2c) can be written as

$$\kappa_{ij}\theta_{,ij} = \theta_s(\lambda_{kl}\dot{\varepsilon}_{kl} + p_k\dot{E}_k + \alpha_v\dot{\theta}) + \Phi_t. \tag{5}$$

The hydrogen diffusion process in piezoelectrics can be described by the Cahn–Hilliard equation in which the hydrogen flux (J) is expressed in terms of the gradient of chemical potential (μ) [15,16],

$$J_i = -\frac{c(r,t)}{R\theta} d_0 \mu_{,i}, \tag{6}$$

where $c(\boldsymbol{r}, t)$ denotes the hydrogen concentration at position vector $\boldsymbol{r}$ and at time t; μ is the chemical potential of hydrogen; d_0 is the diffusivity of hydrogen in an isotropic material, and R is the universal gas constant.

The hydrogen mass balance is given by

$$c_{,t} = -J_{i,i}. \tag{7}$$

The electro-transport and thermo-transport processes, which arise in the presence of electric current and temperature gradients, respectively, can be taken into account in the present model. Details of the consideration of the chemical potential of hydrogen and driving forces due to electro-transport and thermo-transport processes are presented in Appendix A. The diffusion governing equation for hydrogen including chemical potential, electric field and temperature gradients can be obtained by substituting Eq. (16) into Eq. (7). The final governing equation can be expressed as

$$c_{,t} = \frac{cd_0}{R\theta}\left[\mu_{,ii} + eZ^*\phi_{,ii} + \frac{Q^*}{\theta}\theta_{,ii}\right] + \frac{d_0}{R}\left[\left(\frac{c}{\theta}\right)_{,i}\left(\mu + eZ^*\phi\right)_{,i}\right] + \frac{d_0 Q^*}{R}\left[\left(\frac{c}{\theta^2}\right)_{,i}\theta_{,i}\right]. \tag{8}$$

The relevant boundary conditions are

$$c = \bar{c} \quad \text{or} \quad J_n = n \cdot \nabla\mu = 0, \tag{9}$$

where $\bar{c}$ is the specified concentration on the boundary Γ.

3 Numerical solution scheme

A finite element formulation based on the weighted residual method is applied to solve the fully coupled governing equations (1)–(3) for mechanical, thermal and electric fields [18]. The structure of the diffusion governing equation (8) is nonlinear. The explicit Euler finite difference method (FDM) [19] is convenient for the solution of the diffusion equation. The governing equations for hydrogen diffusion and thermo-electromechanical fields are solved separately in each time step. The solutions for hydrogen concentration obtained from the diffusion analysis are used to determine d_{33} based on the experimental data (Fig. 2) [6]. The calculated space-time variation of piezoelectric properties is then supplied as input to the finite element model to determine the thermo-electromechanical field. The updated thermo-electromechanical field is then fed into the FD model to determine the hydrogen concentration at the next time step. This process is repeated over the desired time span to obtain the time histories of hydrogen, thermal, electrical and mechanical fields.

3.1 Finite element formulation of thermo-electromechanical response

The mechanical displacement u, electric potential ϕ, and temperature θ are chosen as nodal degrees of freedom for each element. Using the governing equations presented in the preceding section and applying the weighted residual method [18], the following coupled finite element equations are obtained:

$$\begin{bmatrix} 0 & 0 & 0 \\ 0 & 0 & 0 \\ \theta_0 K_{\theta u} & -\theta_0 K_{\theta\phi} & \theta_0 H_{\theta\theta} \end{bmatrix} \begin{Bmatrix} \dot{u} \\ \dot{\phi} \\ \dot{\theta} \end{Bmatrix} + \begin{bmatrix} K_{uu} & K_{u\phi} & -K_{u\theta} \\ K_{\phi u} & -K_{\phi\phi} & K_{\phi\theta} \\ 0 & 0 & K_{\theta\theta} \end{bmatrix} \begin{Bmatrix} u \\ \phi \\ \theta \end{Bmatrix} = \begin{Bmatrix} F_u \\ F_\phi \\ F_\theta \end{Bmatrix}, \tag{10}$$

where

$$\begin{aligned}
H_{\theta\theta} &= \int_\Omega \alpha_v N_\theta^T N_\theta d\Omega, \quad K_{uu} = \int_\Omega B_u^T C B_u d\Omega, \quad K_{u\theta} = K_{\theta u}^T = \int_\Omega B_u^T \lambda N_\theta d\Omega, \\
K_{\phi\theta} &= K_{\theta\phi}^T = \int_\Omega B_\phi^T p N_\theta d\Omega, \quad K_{u\phi} = K_{\phi u}^T = \int_\Omega B_u^T e B_\phi d\Omega, \\
K_{\theta\theta} &= \int_\Omega B_\theta^T \kappa^T B_\theta d\Omega + \int_\Gamma h_v N_\theta^T N_\theta d\Gamma, \quad F_u = \int_\Omega N_u^T b d\Omega + \int_\Gamma N_u^T \bar{t} d\Gamma, \\
F_\phi &= -\int_\Omega N_\phi^T \Phi_e d\Omega - \int_\Gamma N_\phi^T \bar{Q} d\Gamma, \quad F_\theta = \int_\Omega \Phi_e N_\theta^T d\Omega + \int_\Gamma \bar{q} N_\theta^T d\Gamma + \int_\Gamma h_v N_\theta^T (\theta_f - \theta_s) d\Gamma.
\end{aligned} \tag{11}$$

In addition, N_u, N_ϕ and N_θ are the interpolation matrices containing shape functions for displacement u, electric potential ϕ and temperature θ, respectively; B_u, B_ϕ and B_θ are interpolation matrices for strain, electric field and heat flux, respectively, based on Eq. (3); and the superscript T denotes the transpose of a matrix.

3.2 Finite difference formulation of hydrogen diffusion

Let $c_{i,j}^n$ denotes the hydrogen concentration at point (x_i, y_j) at time t^n. The finite difference version of the diffusion Eq. (8) can be written as

$$\begin{aligned}\frac{c_{i,j}^{n+1}-c_{i,j}^n}{\Delta t} = \frac{d_0 c_{i,j}^n}{R\theta_{i,j}^n}\Bigg[&\frac{\mu_{i+1,j}^n-2\mu_{i,j}^n+\mu_{i-1,j}^n}{(\Delta x)^2}+\frac{\mu_{i,j+1}^n-2\mu_{i,j}^n+\mu_{i,j-1}^n}{(\Delta y)^2}+eZ^*\Bigg\{\frac{\phi_{i+1,j}^n-2\phi_{i,j}^n+\phi_{i-1,j}^n}{(\Delta x)^2}\\&+eZ^*\frac{\phi_{i,j+1}^n-2\phi_{i,j}^n+\phi_{i,j-1}^n}{(\Delta y)^2}\Bigg\}+\frac{Q^*}{\theta_{i,j}^n}\Bigg\{\frac{\theta_{i+1,j}^n-2\theta_{i,j}^n+\theta_{i-1,j}^n}{(\Delta x)^2}+\frac{\theta_{i,j+1}^n-2\theta_{i,j}^n+\theta_{i,j-1}^n}{(\Delta y)^2}\Bigg\}\Bigg]\\&+\frac{d_0}{4R(\Delta x)^2}\left(\frac{c_{i+1,j}^n}{\theta_{i+1,j}^n}-\frac{c_{i-1,j}^n}{\theta_{i-1,j}^n}\right)\left[\left(\mu_{i+1,j}^n-\mu_{i-1,j}^n\right)+eZ^*\left(\phi_{i+1,j}^n-\phi_{i-1,j}^n\right)\right]\\&+\frac{d_0}{4R(\Delta y)^2}\left(\frac{c_{i,j+1}^n}{\theta_{i,j+1}^n}-\frac{c_{i,j-1}^n}{\theta_{i,j-1}^n}\right)\left[\left(\mu_{i,j+1}^n-\mu_{i,j-1}^n\right)+eZ^*\left(\phi_{i,j+1}^n-\phi_{i,j-1}^n\right)\right]\\&+\frac{d_0 Q^*}{4R}\Bigg[\frac{1}{(\Delta x)^2}\left(\frac{c_{i+1,j}^n}{\left(\theta_{i+1,j}^n\right)^2}-\frac{c_{i-1,j}^n}{\left(\theta_{i-1,j}^n\right)^2}\right)\left(\theta_{i+1,j}^n-\theta_{i-1,j}^n\right)\\&+\frac{1}{(\Delta y)^2}\left(\frac{c_{i,j+1}^n}{\left(\theta_{i,j+1}^n\right)^2}-\frac{c_{i,j-1}^n}{\left(\theta_{i,j-1}^n\right)^2}\right)\left(\theta_{i,j+1}^n-\theta_{i,j-1}^n\right)\Bigg],\end{aligned}\tag{12}$$

where Δx and Δy denote the distance intervals between grid points; Δt denotes the time interval, $\Delta t = t^{n+1}-t^n$ and $\mu_{i,j}^n = R\theta_{i,j}^n \ln\frac{c_{i,j}^n}{1-c_{i,j}^n}$.

In Eq. (12), the temperature $\left(\theta_{i,j}^n\right)$ and electric potential $\left(\phi_{i,j}^n\right)$ at grid point (x_i, y_j) at time step t^n are obtained from the FE analysis and supplied to the FD analysis as known values. With the boundary conditions given by Eq. (9), the system of Eqs. (12) can be solved for the unknown $c_{i,j}^{n+1}$ at time t^{n+1}.

3.3 Model validation and 3D analysis using COMSOL Multiphysics®

The solution of the nonlinear diffusion Eq. (12) using FD and the thermo-electromechanical FE equations (10) (also nonlinear due to the dependence of d_{33} on concentration) is computationally expensive for 3D problems. It is therefore attempted to estimate the accuracy of a 2D plane stress model for practical applications. First, the FD–FEM model described in Sects. 3.1 and 3.2 was implemented for the 2D plane stress case. A 2D plane stress model with reduced coupling was also developed by using the 'Equation Based Modelling' capability in *COMSOL Multiphysics*® to compare with the results obtained from the 2D coupled plane stress model described in Sects. 3.1 and 3.2. The *COMSOL Multiphysics*® model provides a simultaneous solution of a thermo-electromechanical continuum subjected to Fickian diffusion. It should be noted that in the Fickian diffusion, movement of hydrogen species is assumed to be driven only by the concentration gradients and the effects of thermo-transport, electro-transport or any other forces (Sect. 2) are neglected. For 3D analysis, a separate model was developed by using the 'Equation Based Modelling' capability of *COMSOL Multiphysics*® [20].

4 Numerical results and discussion

A computer code based on the FD–FE formulation presented in the preceding section was developed. A 2D plane stress four-node isoparametric finite element with four degrees of freedom per node (two displacements, temperature and electric potential) was implemented for thermo-electromechanical analysis. The generalized

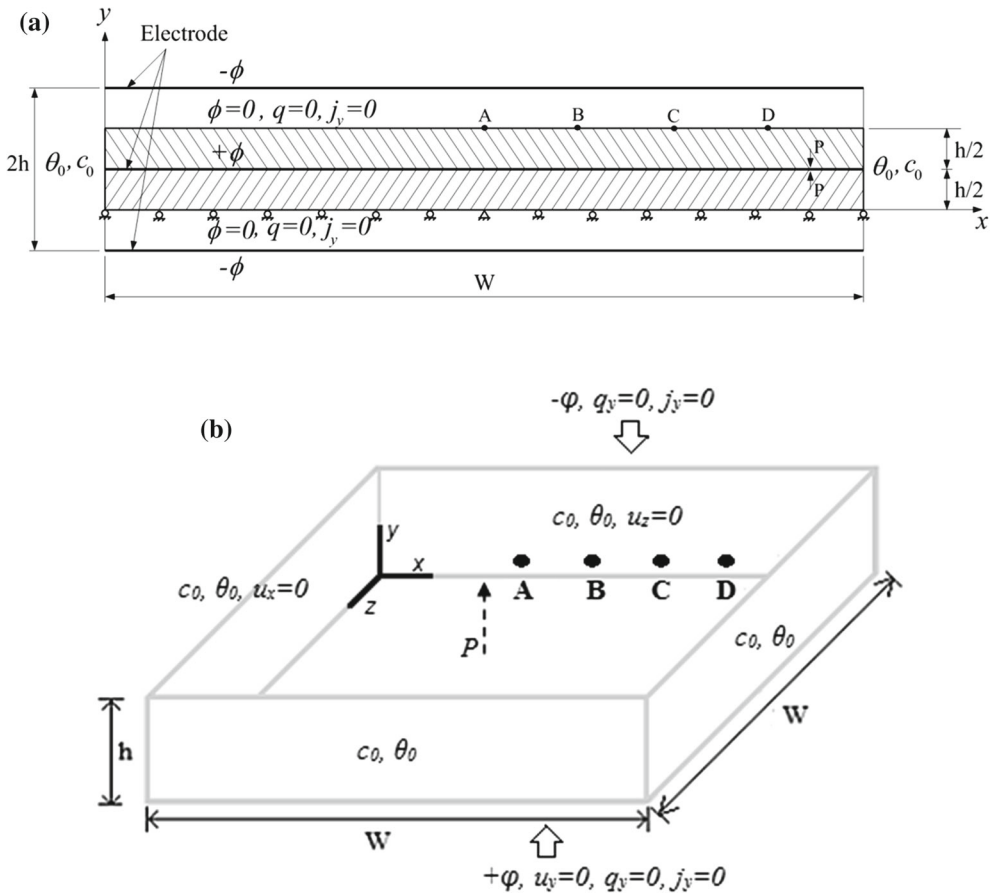

Fig. 3 Geometry, polarization direction, boundary conditions and location of analysis points in **a** 2D plane stress model; and **b** 3D model of a single layer of PZT-based stack actuator

stiffness matrices and load vectors are evaluated by using Gaussian quadrature [21]. The Newmark time integration method [18] is used to solve Eq. (10). Numerical solutions of FD model presented in this paper correspond to $\Delta x = 1.25 \times 10^{-3}$ m, $\Delta y = 2.5 \times 10^{-4}$ m with time interval $\Delta t = 5$ s. The same time interval is used in the finite element analysis.

In this section, the hydrogen diffusion and thermo-piezoelectric response of an idealized single unit cell of a stack actuator composed of adjacent discs as shown in Fig. 3a is simulated. The polarization direction of the adjacent PZT discs is opposite as indicated by an arrow with P. Due to symmetry, only half of each stack is modelled as represented by the shaded area. The thickness of a single layer is $h = 1.0$ mm, and the width (w) is $=10$ mm. Each stack is subjected to 250 V. The top and bottom surfaces are grounded (i.e. $\phi = 0$) due to voltage anti-symmetry and are assumed adiabatic (i.e. $q = 0$) with zero hydrogen flux ($j_y = 0$). Uniform hydrogen concentration (c_0) and temperature (θ_0) are assumed along the left and right surfaces. Mechanical displacement boundary conditions are also shown in Fig. 3a. The piezoelectric material is assumed to have an initial temperature same as the reference temperature $\theta_s = 20\,^{\circ}$C and an initial zero hydrogen concentration.

The stacks are made from a PZT ceramic material which exhibits hexagonal symmetry resulting in transversely isotropic material properties. In order to simulate the plane stress behaviour, it is necessary to convert the 3D constitutive matrix to the appropriate form of the 2D plane stress material coefficient matrices [22]. The plane stress properties of the PZT material after applying the relevant conversions are as follows: piezoelectric coefficients, $e_{31} = -2.29, e_{33} = 17.88, e_{15} = 12.7\,\mathrm{C/m^2}$; elastic constants, $c_{11} = 9.54 \times 10^{10}, c_{13} = 3.27 \times 10^{10}, c_{33} = 7.53 \times 10^{10}, c_{44} = 2.56 \times 10^{10}\,\mathrm{N/m^2}$; pyroelectric constant, $p_n = 2.5 \times 10^{-5}\,\mathrm{C/m^2/K}$; thermal expansion and thermal conductivity, $\alpha = 1.2 \times 10^{-6}/^{\circ}\mathrm{C}, \kappa = 0.17\,\mathrm{W/m/^{\circ}C}$; specific heat at constant volume, $C_v = 420\,\mathrm{J/kg\,^{\circ}C}$; density, $\rho = 7{,}600\,\mathrm{kg/m^3}$; relative permittivity at constant strain, $\varepsilon_{xx} = 728.5, \varepsilon_{yy} = 656.7$; and diffusion coefficient, $d_0 = 1.1 \times 10^{-9}\,\mathrm{m^2/s}$.

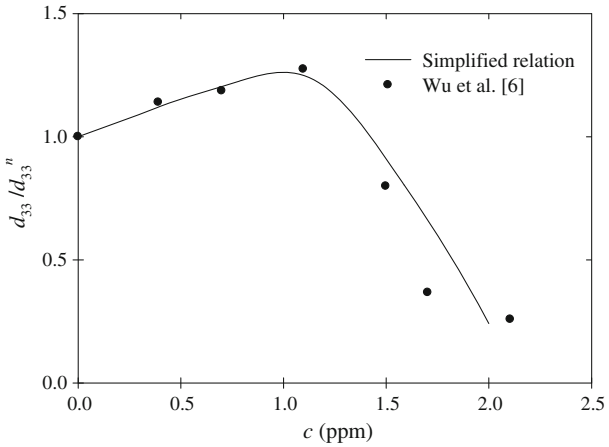

Fig. 4 Model for dependence of d_{33} with hydrogen concentration [6]

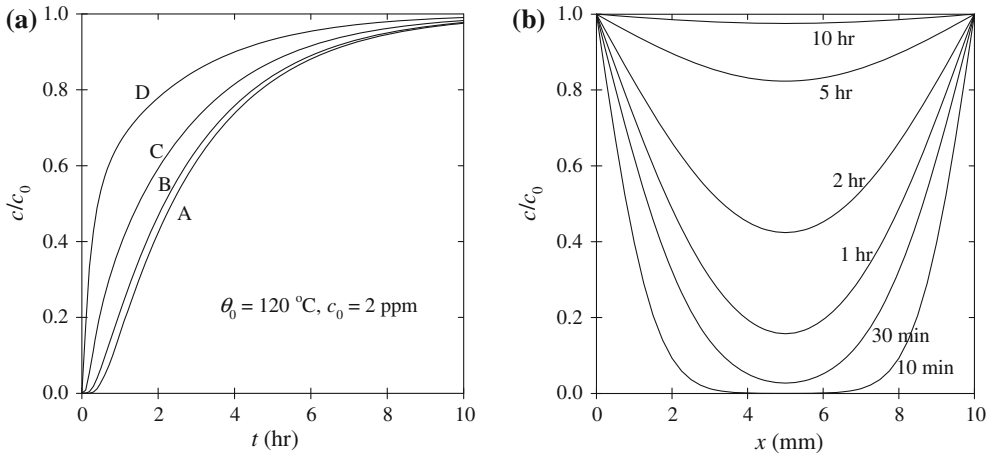

Fig. 5 Hydrogen concentration profile in unit cell from 2D model. **a** Time histories at points *A*, *B*, *C* and *D*; and **b** profiles along the center of the unit cell ($y = h/2$) at different times

Although hydrogen can affect all piezoelectric material properties, attention is given only to d_{33} in the absence of comprehensive experimental data for hydrogen dependence of other piezoelectric and dielectric constants. This is reasonable as the stroke of an actuator is primarily controlled by d_{33}, and there is no significant mechanical loading on the actuator. The experimental results of Wu et al. [6] are utilized in the present modelling and approximated by a smooth curve as shown in Fig. 4 where d_{33}^{n} is the piezoelectric constant of piezoceramic unexposed to hydrogen. Note that the piezoelectric constitutive relation has to be converted from the *e*- to *d*-form [17] to utilize the experimental results in Fig. 4.

A selected set of numerical solutions is presented in Figs. 5, 6, 7 and 8 to examine the response of a unit cell. Due to the applied voltage, the cell has a constant electric field E_y of 500 kV/m on the upper layer and a constant electric field of -500 kV/m on the lower layer. The electric field E_x is practically zero in a piezo actuator. Solutions for hydrogen distribution in the unit cell at various times are presented in Fig. 5 for the case of $\theta_0 = 120\,^{\circ}\mathrm{C}$ and $c_0 = 2.0$ ppm. Figure 5a shows the time histories of hydrogen content at points A, B, C and D (see Fig. 3a). The profiles of hydrogen content along the centre of the unit cell (i.e. along the x direction at $y = h/2$) at different times are shown in Fig. 5b. It can be seen from Fig. 5a, b that steady state is reached by $t = 10$ h. As expected, the hydrogen concentration at points closer to the exposed surface (such as D) increases rapidly with time and the mid-region of unit cell receives a noticeable amount of hydrogen only after some time. These results imply that an actuator might not reach steady-state diffusion state under normal operation condition of an injector except in cases where the exposure takes over a period more than 5 h. Experiments confirm that hydrogen absorbed into PZT diffuses away into atmosphere once a sample is removed from hydrogen environment. Therefore in practical situations, a piezo actuator in a hydrogen fuel

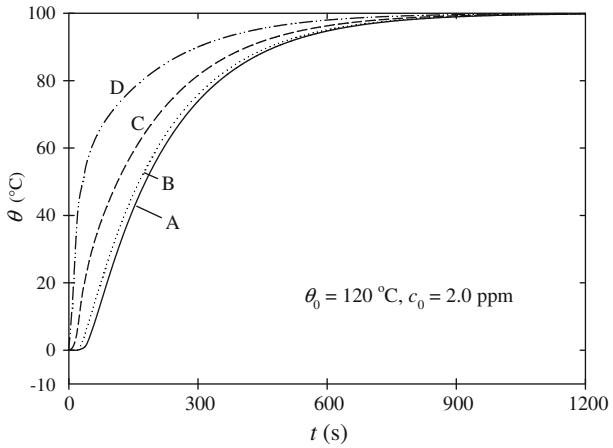

Fig. 6 Temperature profiles at different points in unit cell from 2D model

injector could be subjected to many cycles of hydrogen exposure each lasting a few hours but diffusion steady state may be not be reached during such cycling.

Figure 6 presents the time histories of temperature at points A, B, C and D for the case of $\theta_0 = 120\,^{\circ}\mathrm{C}$ with an initial temperature of 20 °C and $c_0 = 2.0$ ppm. It is noted that under normal operating conditions, a fuel injector gets heated to around 100 °C. The solutions in Fig. 6 indicate that an actuator rapidly gets heated and steady state is reached in about 15 min which is much faster than the time to reach steady-state diffusion. Thus, the effect of temperature gradient on hydrogen diffusion process as shown in Eq. (8) is effective only at the early stage of hydrogen diffusion. As time progresses, the diffusion is controlled primarily by the gradient of hydrogen concentration. The temperature time histories for other values of θ_0 show behaviour similar to that in Fig. 6.

Of importance to the study of fuel injectors is the stroke of an actuator. Vertical displacement u_y at different points along the upper layer of the unit cell is shown in Figs. 7 and 8 for $c_0 = 1.0$ and 2.0 ppm, respectively. The solutions are presented for $\theta_0 = 40$, 80 and 120 °C. The resultant stroke of a stack actuator can be calculated by multiplying the total number of unit cells by the average total displacement of a single cell. The displacements of a cell unexposed to hydrogen are also presented in Figs. 7 and 8 for comparison.

It is evident from Figs. 7 and 8 that the presence of hydrogen has a significant influence on the deformation of unit cell. The displacement histories of a unit cell unexposed to hydrogen show time dependence only during the initial 15–20 min and this essentially represents the thermal expansion of the unit cell as it gets heated. The stroke increases due to temperature is approximately 16.5, 49.4 and 82.4 % of the stroke due to voltage at $\theta_0 = 40$, 80 and 120 °C, respectively, in Figs. 7 and 8. The base temperature is taken as 20 °C. In the case of a unit cell exposed to $c_0 = 1.0$ ppm of hydrogen, the stroke increases gradually with time reaching steady state after about 8 h. The steady-state stroke increases due to hydrogen diffusion is about 26.1 % of the stroke due to voltage. Unlike in the case of an unexposed cell, the cross-sectional displacement profile of a cell exposed to hydrogen is not uniform for nearly 4 h. This is due to slow diffusion of hydrogen and the dependence of d_{33} on hydrogen concentration as shown in Figs. 2 and 4. In the case of Fig. 7, the presence of hydrogen causes an increase in stroke since the concentration throughout the cell remains below 1.0 ppm and according to the Figs. 2 and 4, d_{33} increase with hydrogen concentration when $0.0 < c < 1.0$.

However, in the case of a unit cell exposed to a relatively high concentration of hydrogen ($c_0 = 2.0$ ppm), the stroke shows more complex time histories. As hydrogen diffuses into the material, the displacement initially increases with time, but this increase is more non-uniform across a cross section compared to the case of $c_0 = 1.0$ ppm and the peak displacement at various points occurs at substantially different time instances as a result of the diffusion process. For example, around $t = 2.5$ h, the displacement of the central region is over 30 % of the displacement near the exposed surface of unit cell. Such displacement non-uniformity might enhance electrode delamination in an injector actuator under repeated cycles of hydrogen exposure. The complex time histories observed in Fig. 8 are a direct result of the nature of d_{33} variation with hydrogen concentration as shown in Figs. 2 and 4. Unlike the case shown in Fig. 7, the hydrogen concentration at points in the unit cell increases beyond 1.0 ppm and in this region d_{33} decreases with increasing concentration (Figs. 2, 4). The actuator stroke therefore shows a significant decrease with time as the hydrogen concentration at internal points increase beyond

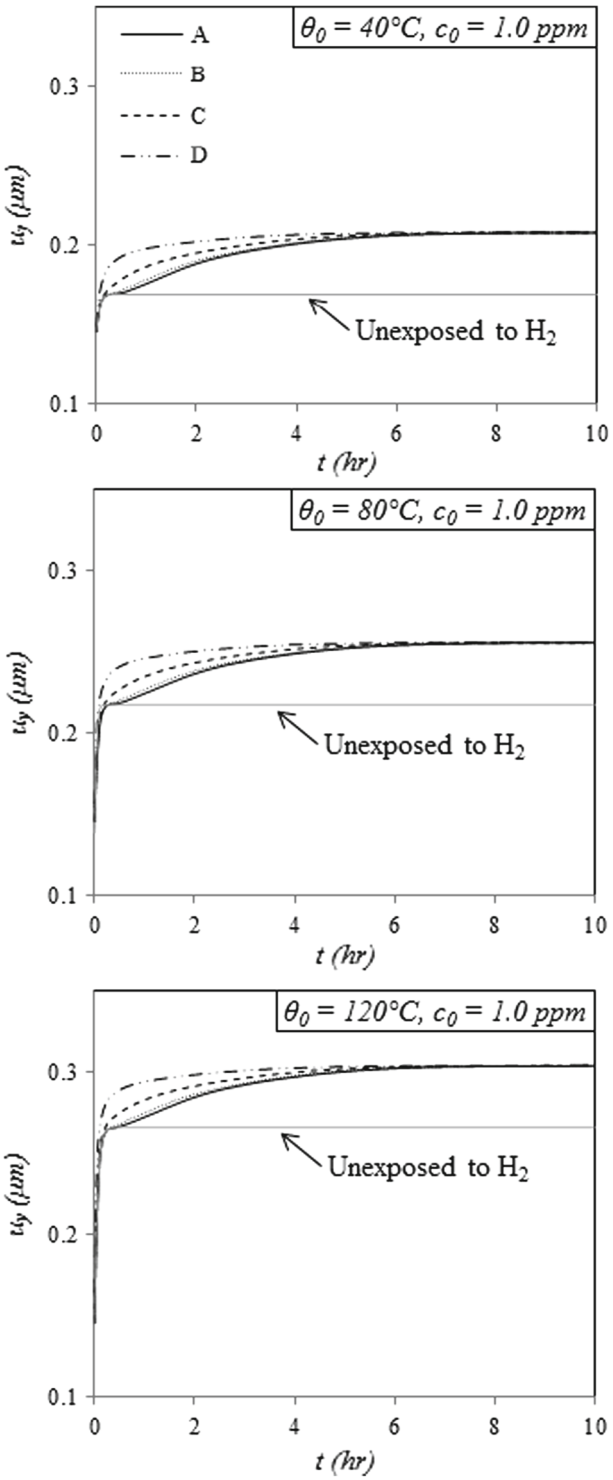

Fig. 7 Vertical displacement profiles at different points in unit cell ($c_0 = 1.0$ ppm) from 2D plane stress model

1.0 ppm. The final steady stroke can be substantially smaller than that of an unexposed actuator. This can have a significant effect on the performance of an injector as well as an engine. It is therefore important to have a thorough understanding of the dependence of properties of piezoelectric materials on hydrogen concentration to develop actuators for injectors that can perform well under different operating conditions. The current

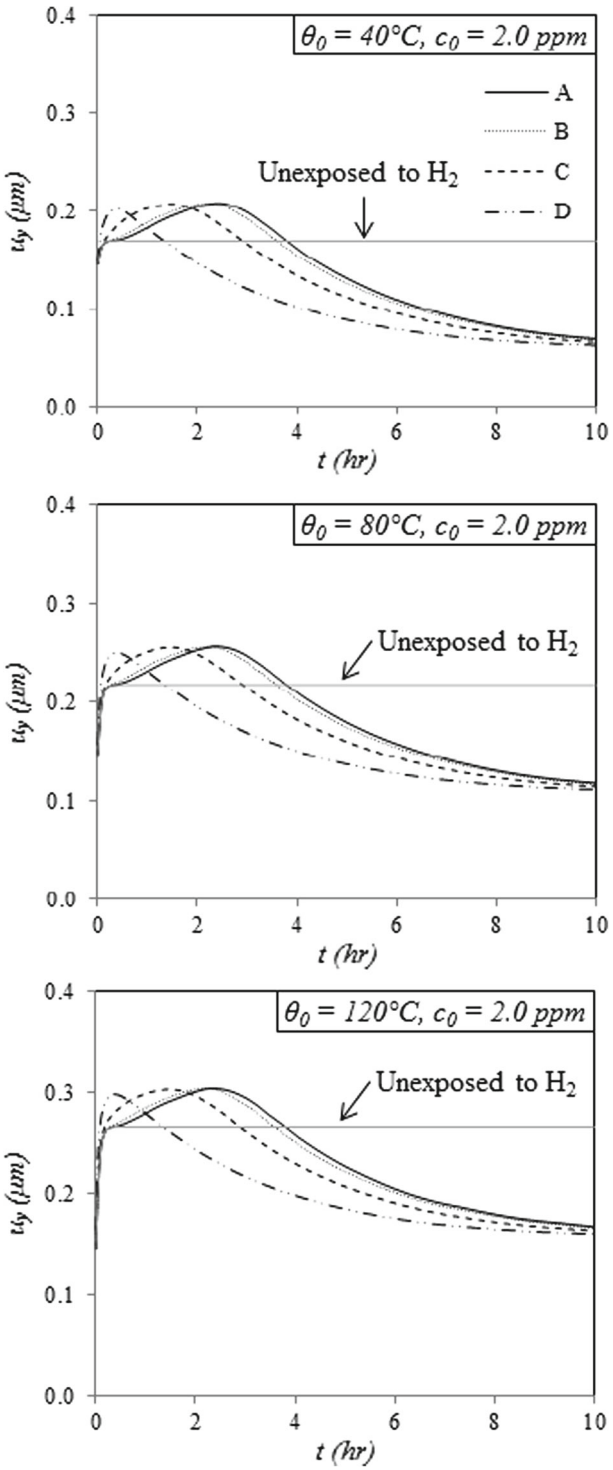

Fig. 8 Vertical displacement profiles at different points in unit cell from 2D plane stress model ($c_0 = 2.0$ ppm)

numerical results also suggest that development of coatings and other hydrogen containment technologies to ensure minimum diffusion of hydrogen (very low concentration) into an injector is an important direction for future research.

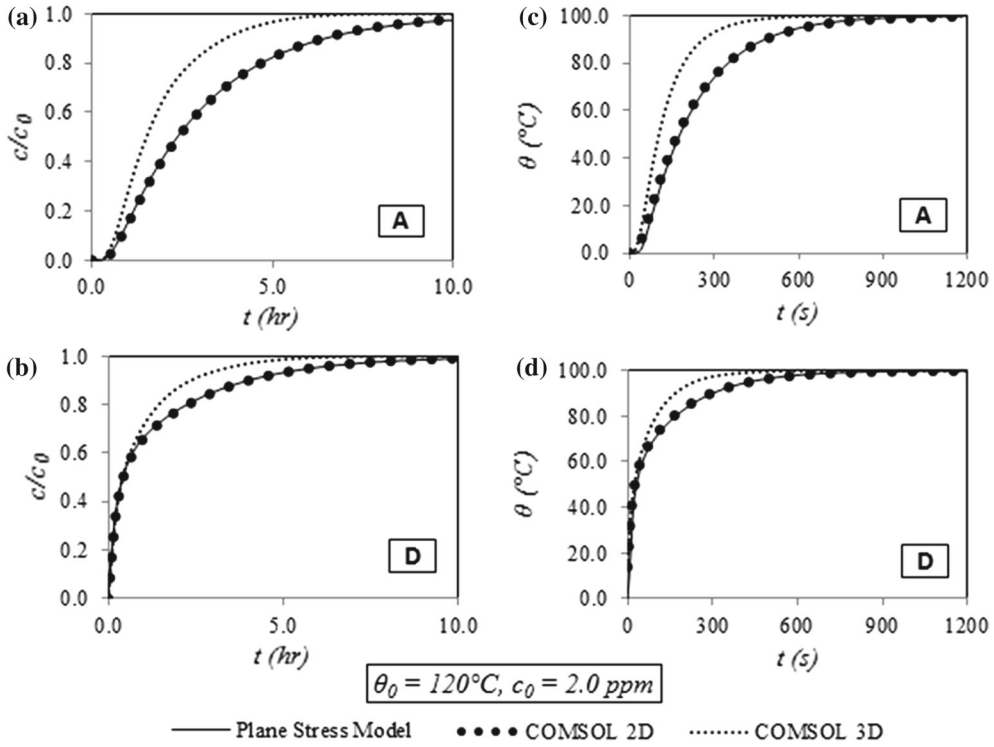

Fig. 9 Comparison of results from different models for the time histories of hydrogen concentration (**a**, **b**) and temperature (**c**, **d**) at points A and D

5 Comparison with Comsol® results

As the conditions of an actuator in a practical situation are three dimensional, the applicability of the 2D plane stress model to study 3D response is investigated. In order to perform a 3D analysis, a single layer of the stack actuator with electrodes on the top and bottom surfaces is modelled as shown in Fig. 3b. This model is assumed to have a depth of $W = 10\,\text{mm}$ in z direction, which is same as the width of the 2D plane stress model described earlier in Sect. 4. The layer thickness $h = 1\,\text{mm}$ is also the same in both the models. The initial and boundary conditions are kept consistent with those mentioned in the 2D plane stress model. It should be noted that in the 3D model, boundary concentration c_0 and temperature θ_0 are present on the four lateral surfaces. This would generate diffusion and heat fluxes in two directions (x, z). The material of the 3D layer is same as that of the 2D plane stress model, exhibiting hexagonal symmetry and having properties [22] that are transversely isotropic about y axis.

The governing equations for the thermo-electromechanical material behaviour (Eq. 1) and the time-dependent diffusion (Eq. 7) are simultaneously solved for the fundamental state variables ($u_x, u_y, u_z, \varphi, \theta$ and c) using the 'Equation Based Modelling' feature of *COMSOL Multiphysics*®. As mentioned earlier, the diffusion of hydrogen into PZT is assumed to be driven only by the hydrogen concentration gradient. A 3D, 4-node tetrahedral element with six degrees of freedom per node is used in the modelling. Upon conducting a mesh-dependence analysis, a 'normal' mesh with 1,476 elements is chosen to run all test cases. The in-built 'Time- Dependent Solver' is used to generate the solution at time intervals of $\Delta t = 5\,\text{s}$. In the 3D geometry, the analysis points A, B, C and D are located in the mid-plane ($z = 5\,\text{mm}$) and at equivalent positions (x, y) with respect to the 2D model shown in Fig. 3a.

To compare with the 2D plane stress model described in Sect. 4, another 2D plane stress model but with reduced coupling is developed using the 'Equation Based Modelling' feature of *COMSOL Multiphysics*®. A 2D, 3-node triangular element with five degrees of freedom per node is used to mesh the geometry with 608 elements. The time interval $\Delta t = 5\,\text{s}$ is same as that in the other FD-FE model.

Figure 9 shows a comparison of results from various models developed during this study for hydrogen concentration and temperature evolution. Clearly, the results from the 2D plane stress model described in Sect. 4 match very closely with those obtained from a similar 2D model developed in COMSOL. This implies

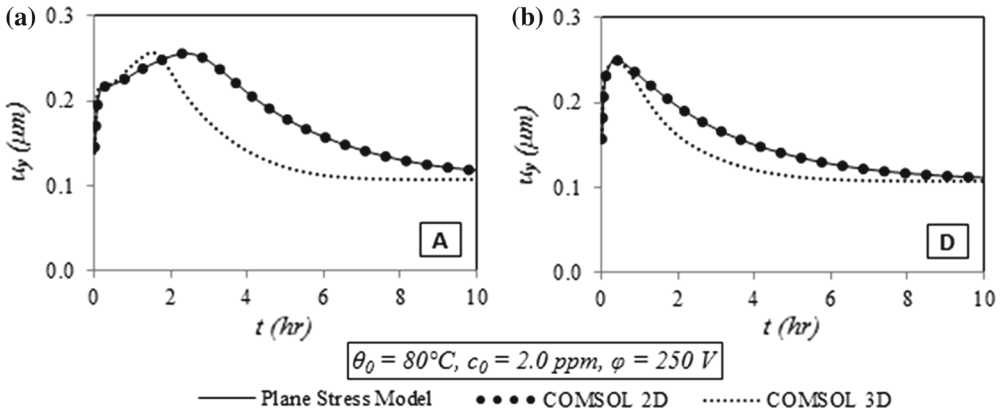

Fig. 10 Comparison of results from different models for the time histories of vertical displacement u_y at points A and D

that thermo-transport and electro-transport effects in diffusion are negligible and Fickian diffusion is the main driving force. The results confirm that the technique of sequentially solving the thermo-electromechanical equations (FE) and diffusion equation (FD) is as effective in the present problem as solving a simultaneous 'thermo-electromechanical + diffusion' system. As mentioned earlier, a 3D model is a more complete representation of the operating environment in which an actuator layer is exposed to ambient temperature and hydrogen concentration on four lateral surfaces (Fig. 3b). These conditions result in the thermal and diffusion fluxes being produced in two directions (x, z). Therefore, all points within the 3D geometry experience greater thermal and diffusion contributions and reach a steady state more quickly than in a 2D case. This is reflected in the results from the 3D COMSOL model in Fig. 9.

The vertical displacements u_y from various models are shown in Fig. 10. The variations of displacement profiles between different models resemble those for the concentration time histories in Fig. 9. Both 2D and 3D models predict same peak vertical displacements. However, due to the differences in concentration time histories between 2D and 3D models, the peak displacement and the final steady state displacement condition are achieved at different time instances. It is clear from the results shown in Figs. 9 and 10 that the 2D plane stress model accurately captures the key features of diffusion as well as displacement response of an actuator. From a computational point of view, the 2D model is far more efficient that the 3D case.

6 Application to a practical case

In the previous sections, the piezoelectric strain coefficient d_{33} has been treated as a function of hydrogen concentration c. In addition to this, experiments have reported the d_{33} value to be also dependent on longitudinal electric field E_3 and temperature rise θ [11,12,20]. Performance of piezoelectric stack actuators developed by *PI Ceramic GmbH* of Germany was experimentally investigated by Singh [20]. These actuators have dimensions of 5.00 × 5.00 × 0.05 mm resulting in a layer thickness to width ratio (h/W) of 1 % and are currently used by industry for fuel injector applications. According to the experimental results of Singh [20], d_{33} is constant for up to 20 V beyond which its starts increasing with the applied voltage giving rise to nonlinear behaviour. This behaviour of d_{33} can be easily seen from Fig. 11 where the experimentally observed stroke–voltage relationship of a PI stack actuator is presented. The 2D plane stress model, described in Sect. 4, is used to predict this behaviour by making use of variable d_{33} values for different applied voltages as reported by Singh [20]. Comparison of results from the numerical model and the experiments is presented in Fig. 11 for a quasi-static voltage applied at 20 °C. The stroke results from the 2D model are in complete agreement with the experiments that demonstrate the model's accuracy. It should be noted that solutions in Fig. 11 correspond to an actuator unexposed to hydrogen. For the actuators tested by Singh [20], very minor variation in stroke with ambient temperature was observed within 5–80 °C, the temperature range typical of a fuel injector. Therefore, the value of d_{33} was assumed to be constant with temperature.

The 2D plane stress model, which was developed during the present work, is customized to run a test case for the *PI Ceramic*® actuator to simulate a static operation at 100 V applied voltage, 20 °C ambient temperature and 2 ppm surface hydrogen concentration. The d_{33} is assumed to be a function of both concentration (as per Wu et al. [6]) and applied voltage (as per Singh [20]), and the value at zero hydrogen concentration was

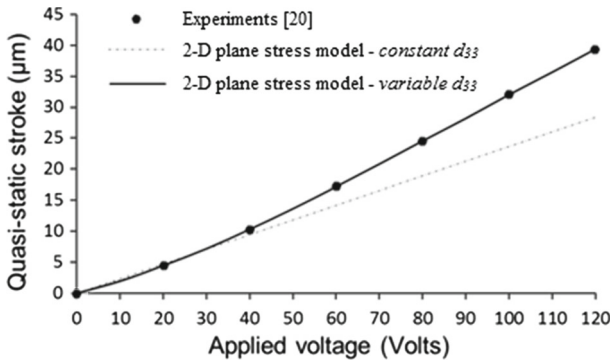

Fig. 11 Comparison of experimental [20] and 2D plane stress model stroke-voltage relationship at 20 °C for an unexposed *PI Ceramic*® actuator

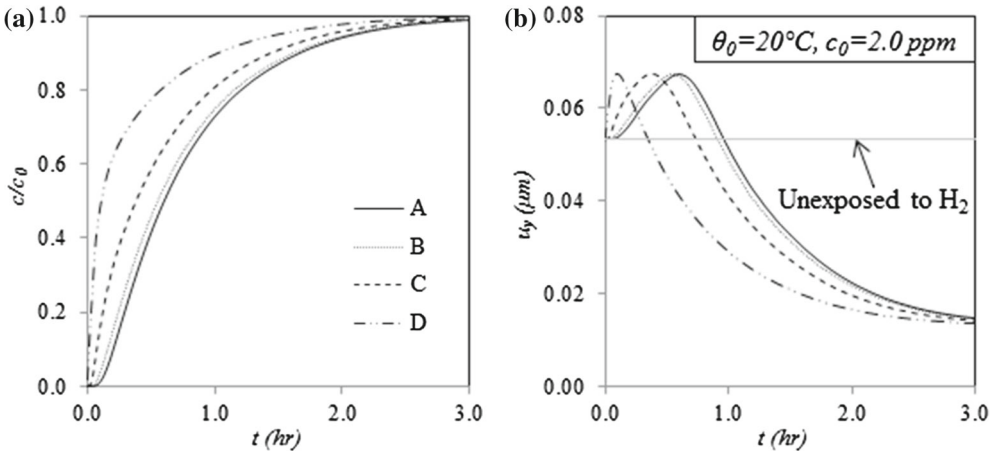

Fig. 12 Time histories for (**a**) hydrogen concentration; and (**b**) vertical displacement of a *PI Ceramic*® actuator subjected to a static voltage of 100 V from 2D plane stress model

obtained from the experiments. Four points A, B, C and D are chosen on the top surface of the actuator layer as shown in Fig. 3a, with the exception that dimensions $W = 5.00$ and $h = 0.05$ mm in this case. Time histories of concentration c and vertical displacement u_y are shown in Fig. 12. When compared with the time histories presented in Sect. 4 (Figs. 5a, 8), it is clear that the trend is very similar. Due to the shorter lateral dimensions of actuator, steady state is attained more quickly in the case of *PI Ceramic*® actuators. Based on this observation, optimum cross-sectional dimensions could theoretically reduce the time period for which an actuator experiences non-uniform displacement across its cross section, thereby reducing the potential for electrode delamination during operation.

7 Conclusions

A 2D plane stress numerical model based on the finite element and finite difference methods is successfully developed to study the fully coupled linear thermo-electro-mechanical fields and nonlinear diffusion in piezoelectric materials exposed to hydrogen. Experimental data on the dependence of piezoelectric coefficient d_{33} of PZT on hydrogen concentration are implemented in the analysis. Selected numerical solutions are presented for temperature profiles, hydrogen concentration distribution and axial deformation of an actuator unit cell. It is found that a typical piezo actuator in an injector gets heated rapidly when subjected to an external temperature increase and the steady state is reached within 15–20 min. The diffusion of hydrogen is relatively slower compared to heating and it could take 2–10 h for an actuator to reach steady-state concentration. It is therefore noted that temperature gradient has an effect on diffusion only during the early stages of diffusion and thereafter the effect of thermo-transport can be neglected.

The actuator stroke is significantly influenced by the presence of hydrogen since its concentration affects d_{33}. At low concentrations ($\leq$1 ppm), the presence of hydrogen may lead to an increase in actuator stroke and that may have a positive effect on injector performance. However, at higher concentrations ($>$1 ppm), the presence of hydrogen can cause significant non-uniform cross-sectional displacements as well as substantially lower steady-state strokes compared to unexposed actuators. This behaviour may have a significant negative impact on the reliability, performance and durability of the actuators. Results from the coupled model are compared with 2D plane stress and 3D models with reduced coupling that were developed using *COMSOL Multiphysics*®. It is found that a 2D plane stress model captures the key features of 3D diffusion and displacement profiles. It is therefore recommended that 2D models can be used in practical situations to maintain computational efficiency. A 2D model is also capable of simulating an actuator with voltage-dependent d_{33} based on comparisons with the experimental results.

Acknowledgments This research was supported by a Grant from the Natural Sciences and Engineering Research Council (NSERC) of Canada.

Appendix A

Following Ma [16], the chemical potential μ of hydrogen can be expressed as

$$\mu = w + \bar{\mu} + R\theta \ln \frac{c(\boldsymbol{r}, t)}{1 - c(\boldsymbol{r}, t)}, \tag{13}$$

where w is related to the interaction energy between interstitial hydrogen and the externally applied stress and $\bar{\mu}$ is the sum of the elastic distortion energy due to hydrogen interstitials, internal energy due to bonding between hydrogen and the matrix, and entropy of vibration.
A preload is usually applied to a PZT actuator to control the tensile stress and strain. In practical cases, the value of preload is small and its influence on the actuator performance is negligible [11,12]. Furthermore, the diffusion process is not significantly affected at low stress levels. The influence of the work done by externally applied load is, therefore, not considered in the present work. In addition, the entropy of vibration and internal energy related to bonding properties between hydrogen and PZT ceramics are independent of position $\boldsymbol{r}$ for uniform temperature and dilute solutions. It is also assumed that elastic interaction between hydrogen atoms and matrix material plays a minor role in the diffusion process, and hence, $\bar{\mu}$ is not considered in the present study to further simplify the model.
The electro-transport and thermo-transport processes, which arise in the presence of electric current and temperature gradients, respectively, are taken into account in the present model. These processes induce a hydrogen flux in addition to that caused by the gradient of hydrogen concentration. The force due to electro-transport is described phenomenologically by an effective charge number Z^* as [23]

$$F_i^E = -eZ^*\phi_{,i}, \tag{14}$$

where e is the elementary charge and $-\phi_{,i}$ is the applied electric field in the i-direction.
The driving force due to a temperature gradient is described by [23]

$$F_i^\theta = -\frac{Q^*}{\theta}\theta_{,i}, \tag{15}$$

where Q^* is the heat transport.
The total flux J_i in Eq. (6) can be modified to include the driving forces F_i^E and F_i^θ corresponding to electro-transport and thermo-transport processes as [24]

$$J_i = -\frac{cd_0}{R\theta}\left[\mu_{,i} + eZ^*\phi_{,i} + \frac{Q^*}{\theta}\theta_{,i}\right]. \tag{16}$$

References

1. Ballato, A.: Piezoelectricity: old effect, new thrusts. IEEE Trans. Ultrason. Ferroelectr. Freq. Control **42**, 916–926 (1995)
2. Heywang, W., Lubitz, K., Wersing, W.: Piezoelectricity: evolution and future of a technology. Springer, Berlin (2008)
3. Chee, C.Y.K., Tong, L., Steven, G.P.: A Review on the modelling of piezoelectric sensors and actuators incorporated in intelligent structures. J. Intell. Mater. Syst. Struct. **9**, 3–19 (1998)
4. Schuh, C., Steinkopff, T., Wolff, A., Lubitz, K.: Piezoceramic multilayer actuators for fuel injection systems in automotive area. Proc. SPIE **3992**, 165–175 (2003)
5. Fujii, A., Toyao, T.: Piezoelectric actuators with high reliability for diesel injection valve. In: Tenth International Conference on New Actuators, pp. 177–180 (2006)
6. Wu, M., Huang, H., Chu, W., Guo, L., Qiao, L., Xu, J., Zhang, T.Y.: Tuning the ferroelectric and piezoelectric properties of $0.91Pb(Zn_{1/3}Nb_{2/3})O_3$-$0.09PbTiO_3$ single crystals and lead titanate ceramics by doping hydrogen. J. Phys. Chem. C **114**, 9955–9960 (2010)
7. Peng, X., Su, Y.J., Gao, K.W., Qiao, L.J., Chu, W.Y.: Hydrogen fissure in PZT ferroelectric ceramic. Mater. Lett. **58**, 2073–2075 (2004)
8. Wang, Y., Chu, W.Y., Qiao, L.J., Su, Y.J.: Hydrogen-induced delayed fracture of PZT ceramics during dynamic charging under constant load. Mater. Sci. Eng. **B98**, 1–5 (2003)
9. ShafieiNickchi, T., Oprea, C., Alfantazi, A., Troczynski, T.: Investigation of hydrogen effects on the properties of Pb(Zr,Ti)O3 in tetragonal phase using water electrolysis technique. J. Appl. Phys. **99**, 212903 (2011)
10. ShafieiOprea, C., Alfantazi, A., Troczynski, T.: In situ monitoring of the effects of hydrogen on Pb(Zr,Ti)O3 structure. J. Appl. Phys. **109**, 114108 (2011)
11. Li, F.X., Rajapakse, R.K.N.D., Mumford, D., Gadala, M.: Quasi-static thermo-electro-mechanical behaviour of piezoelectric stack actuators. Smart Mater. Struct. **17**, 015049 (2008)
12. Senousy, M.S., Li, F.X., Mumford, D., Gadala, M., Rajapakse, R.K.N.D.: Thermo-electro-mechanical performance of piezoelectric stack actuators for fuel injector applications. J. Intell. Mater. Syst. Struct. **20**, 387–399 (2009)
13. Wang, H., Cooper, T.A., Lin, H.T., Wereszczak, A.A.: Fatigue responses of lead zirconate titanate stacks under semibipolar electric cycling with mechanical preload. J. Appl. Phys. **108**, 084107 (2010)
14. Alvine, K.J., Pitman, S., Shutthanandan, V., Vijayakumar, M., Bennett, W., Skorski, D.: Agreement 11754-Hydrogen Materials Compatibility, FY 2011 progress report for Propulsion Materials, US DOE EERE (2012)
15. Cahn, J.W., Hilliard, J.E.: Free energy of a nonuniform system: I interfacial energy. J. Chem. Phys. **28**, 258–267 (1958)
16. Ma, X.Q.: Computer simulation of morphological evolution of hydride in zirconium under applied stress. Ph.D. Thesis, The Hong Kong Polytechnic University (2003)
17. Ikeda, T.: Fundamentals of Piezoelectricity. Oxford University Press, Oxford (1996)
18. Bathe, K.J.: Finite Element Procedures. Prentice Hall, New Jersey (1996)
19. Hoffman, J.D.: Numerical Methods for Engineers and Scientists. McGraw-Hill, Boston (1992)
20. Singh Y.: Experimental investigation and numerical modelling of hydrogen exposed piezoelectric actuators for fuel injector applications. M.A.Sc. thesis, Simon Fraser University (2013)
21. Mathews, J.H., Fink, K.D.: Numerical Methods Using Matlab, 3rd edn. Prentice Hall, New Jersey (1999)
22. Rajapakse, R.K.N.D.: Plane strain/stress solutions for piezoelectric solids. Compos. Part B **28B**, 385–396 (1997)
23. Wipf, H.: Diffusion of hydrogen in metals. In: Wipf, H. (Eds.) Hydrogen in Metals III: Properties and Applications. Springer, Berlin, pp. 51–92 (1997)
24. Clayton, J.D., Chung, P.W., Grinfeld, M.A., Nothwang, W.D.: Continuum modeling of charged vacancy migration in elastic dielectric solids, with application to perovskite thin films. Mech. Res. Commun. **35**, 57–64 (2008)